Homogenization of granular material modeled by a three-dimensional Discrete Element Method

C. Wellmann, C. Lillie and P. Wriggers

Institute of Mechanics and Computational Mechanics,
Leibniz University Hannover,
Hannover, Germany

Abstract

A homogenization strategy for granular materials is presented and applied to a three-dimensional Discrete Element Method (DEM), that uses superellipsoids as particles. Macroscopic quantities are derived from the microscopic quantities resulting from a DEM simulation by averaging over representative volume elements (RVEs). The implementation of a RVE is described in detail regarding the definition and discretization of the RVE boundary. The homogenization strategy is validated by DEM simulations of compression and shear tests of cohesionless granular assemblies. Finally an elasto-plastic material is fit to the resulting stress-strain curves.

Key words: Homogenization, DEM, RVE

1 Introduction

Since the pioneering work of [8] Discrete Element Methods (DEMs) have become the leading computational method for analysing the complex phenomena exhibited by granular materials. They have been applied to many problems in soil and rock mechanics (see [7] for an overview) and are expected to become more important in these fields, when an increase of computer speed and memory makes large-scale DEM simulations feasible ([6]).
Within a DEM the mechanical behavior of granular materials is described in terms of the individual particle's motion and inter-particle contact forces. The process of deriving a continuum mechanical description from this microscopic quantities is called homogenization. In this paper a homogenization strategy, which was used in [10] and [9] in combination with a two-dimensional DEM using Voronoi polygons as particles, is applied to a three-dimensional DEM using superellipsoids as particles. In contrast to the approach in [10] and [9], where an extended continuum model is used for the macroscopic description, a standard continuum is applied here. Hence, no couple stress tensor is needed and the macroscopic quantities of interest, i.e. the strain and stress tensor, are symmetric by definition and as a result of the scale seperation argument respectively. In [16] a similar homogenization approach was applied to a periodic unit cell containing a package of circular discs. Here the periodicity of the boundary particle fluctuations and rotations yields the symmetry of the averaged stresses.
The initial point of the homogenization approach is the introduction of representative volume elements (RVEs), which serve as averaging volumes for the macroscopic quantities. The key assumption of the presented derivation is that the three considered systems, i.e. the macroscopic body, a RVE and a single particle, are defined on different scales, namely the macro-, meso- and microscale, meaning that they are of completely different size. Under this circumstances Hashin's MMM principle of scale separation can be applied, leading to simplified expressions for the volumetric averages of the macroscopic quantities. The stress tensor is related to the outward oriented contact forces of a RVE while the strain tensor is related to the displacements of the boundary particles of a RVE.
Special attention is paid to the numerical implementation of a RVE with respect to the three-dimensional DEM being considered. Particularly a convenient transfer of the definition and discretization of the RVE boundary used in [10] and [9] from the two-dimensional to the three-dimensional case is by no means straightforward. Furthermore the estimation of the correct RVE volume is a non-trivial but important task, since the correct volume is necessary to ensure the comparability of results obtained from different RVE sizes.
The homogenization strategy is then validated by DEM simulations of a compression and a shear test of a cuboid particle sample. Averaged stresses and strains are calculated in the course of the simulations resulting in stress-

strain curves. Thereby, the influence of some DEM parameters on the resulting stresses is analyzed. Finally, the macroscopic behavior exhibited by the particle sample is described in terms of an elasto-plastic material model, namely the Drucker-Prager soil model. Therefor the elastic and plastic parameters are fit to the stress-strain curves of the compression and shear tests.
The paper is organized as follows: Section 2 briefly describes the used DEM. In section 3 the application of the homogenization strategy yields expressions for the average stress and strain. Section 4 deals with the numerical implementation of RVEs. The DEM simulations used for validation are discussed in section 5. Finally, the fitting of the elasto-plastic material is described, followed by a conclusion.

2 Discrete Element Method

Most of todays three-dimensional DEM codes use spherical particles because of the minimum computational effort for contact detection. However, regarding soil mechanics, it is well known that geometries of real soil particles are not well described by spheres, see e.g. [17] and [18]. [20] and [15] compared the behavior of spherical particles with that of ellipsoidal particles in two and three dimensions, and showed that the main problem with spherical particles is their small resistance against rolling. To overcome this problem several other particle shapes have been proposed, e.g. polyhedral particles ([5], [13]), particles that are build of clusters of spheres ([11], [17], [12], [18]), oval particles that are build of arcs ([21], [14]) and particles based on potential functions ([15], [22], [4], [19]). Here superellipsoid particles as proposed in [3] are used, which have a smooth surface and therefore uniquely defined outward normals, what is favorable for calculation of contact forces. Further a superellipsoid allows for arbitrary aspect ratios in three dimensions yielding the desired interlocking phenomena described in [15]. It is described by the geometric potential function (sometimes called inside-outside function)

$$F(\boldsymbol{x}) = \left(\left| \frac{x_1}{a} \right|^{\frac{2}{n}} + \left| \frac{x_2}{b} \right|^{\frac{2}{n}} \right)^{\frac{n}{m}} + \left| \frac{x_3}{c} \right|^{\frac{2}{m}} - 1 \quad \text{with} \quad m, n \in (0, 2) \; . \tag{1}$$

Every point $\boldsymbol{p}$ in three-space belonging to the superellipsoid obeys $F(\boldsymbol{p}) \leq 0$. The parameters a,b and c are the dimensions of the superellipsoid in x_1, x_2 and x_3 direction. The parameters m and n control the roundness of the superellipsoid, compare Fig. 1. Note, that $m, n \to 0$ yields a cuboid and $m, n \to 2$ yields an octahedron. The individual particles are considered as rigid bodies

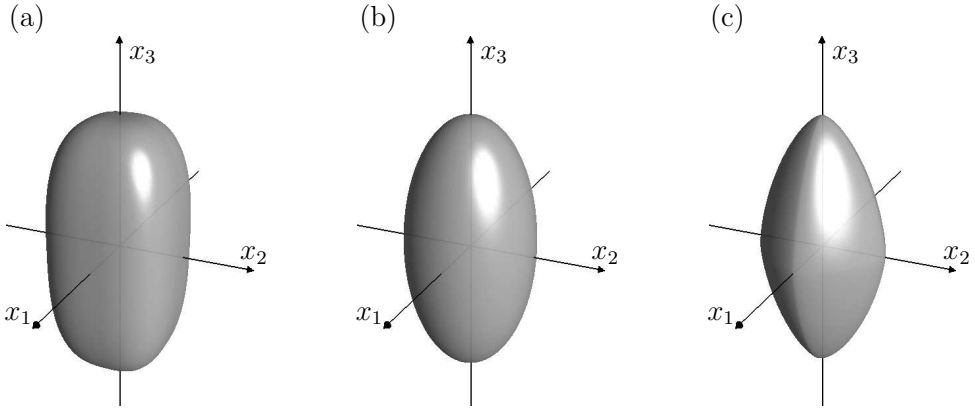

Fig. 1. Superellipsoids with $a = b = c/2$ and $m = n = 0.7$ (a), $m = n = 1$ (b) and $m = n = 1.3$ (c).

with the three translational and three rotational degrees of freedom assigned to their center of mass $\boldsymbol{x}_M$. They interact in terms of contact forces which are calculated by means of a penalty-type formulation. Therefore, a small overlap

of two particles $\mathcal{P}^i$ and $\mathcal{P}^j$ is allowed, compare the two-dimensional sketch in Fig. 2. Herein $\boldsymbol{p}^i$ and $\boldsymbol{p}^j$ are the so called contact points. $\boldsymbol{n}^i$ and $\boldsymbol{n}^j$ are the

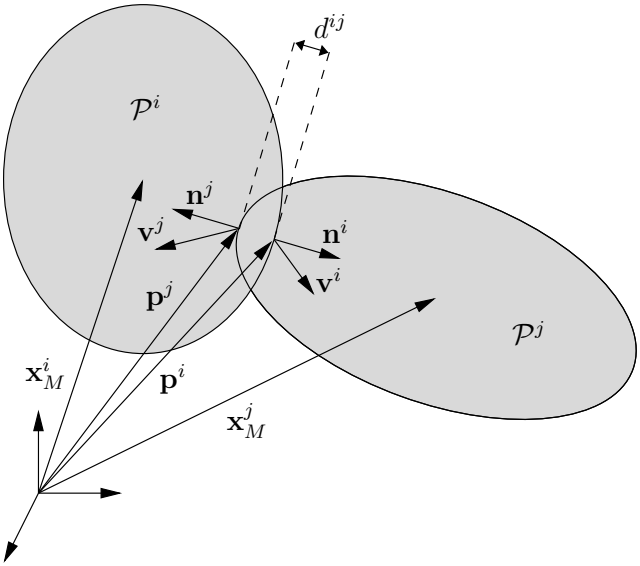

Fig. 2. Two-dimensional sketch of overlapping particles $\mathcal{P}^i$ and $\mathcal{P}^j$.

outward-oriented unit normals, and $\boldsymbol{v}^i$ and $\boldsymbol{v}^j$ denote the velocities of $\boldsymbol{p}^i$ and $\boldsymbol{p}^j$. The contact points are defined as those points on the surfaces of $\mathcal{P}^i$ and $\mathcal{P}^j$ where $\boldsymbol{n}^i = -\boldsymbol{n}^j$ and $\boldsymbol{p}^j = \boldsymbol{p}^i + d^{ij}\,\boldsymbol{n}^j$ holds. d^{ij} is the overlapping distance, which will be used to compute the elastic repulsive force. Hence, the contact force is first split into a normal and a tangential component

$$\boldsymbol{f}^{ij} = \boldsymbol{f}^{(ij)N} + \boldsymbol{f}^{(ij)T} = -f^{(ij)N}\boldsymbol{n}^i + \boldsymbol{f}^{(ij)T}\,. \tag{2}$$

The normal component is calculated by a viscoelastic contact law

$$f^{(ij)N} = c^N d^{ij} + D\left(\boldsymbol{v}^{ij}\cdot\boldsymbol{n}^i\right)\,. \tag{3}$$

The elastic constant c^N is called penalty parameter of the normal contact and $\boldsymbol{v}^{ij} = \boldsymbol{v}^i - \boldsymbol{v}^j$ is the relative velocity of the contact points. In order to get critical damping the damping parameter is chosen as

$$D = 2\sqrt{c^N \frac{m^i\,m^j}{m^i + m^j}}\,, \tag{4}$$

where m^i and m^j denote the masses of $\mathcal{P}^i$ and $\mathcal{P}^j$ respectively. The normal and tangential contact force are coupled by Coulomb's friction law. The tangential component in the actual time-step t is derived from the one in the previous time-step $t-1$ using the friction law

$$\boldsymbol{f}_t^{(ij)T} = \min\left(\mu\,\|\boldsymbol{f}_t^{(ij)N}\|, \|\boldsymbol{f}_{t-1}^{(ij)T} - c^T\Delta t\,\boldsymbol{v}^{(ij)T}\|\right)\frac{\boldsymbol{f}_{t-1}^{(ij)T} - c^T\Delta t\,\boldsymbol{v}^{(ij)T}}{\|\boldsymbol{f}_{t-1}^{(ij)T} - c^T\Delta t\,\boldsymbol{v}^{(ij)T}\|}\,. \tag{5}$$

Herein $\boldsymbol{v}^{(ij)T} = \boldsymbol{v}^{ij} - (\boldsymbol{v}^{ij} \cdot \boldsymbol{n}^i)\, \boldsymbol{n}^i$ is the tangential component of the relative velocity, Δt is the time-step length, c^T denotes the penalty parameter of the tangential contact and μ is the coefficient of friction according to Coulomb.
Additionally to contact damping, global damping forces $\boldsymbol{f}_d^i$ and moments $\boldsymbol{m}_d^i$ are applied to the particles $\mathcal{P}^i$ in order to reach an equilibrium state in minimum time. They are proportional to the velocity of the particle's center of mass $\dot{\boldsymbol{x}}_M^i$ and the rotational velocity $\boldsymbol{\omega}^i$ respectively

$$\boldsymbol{f}_d^i = -\underline{D}^f \cdot \dot{\boldsymbol{x}}_M^i \quad \text{with} \quad \underline{D}^f = \sum_{i=1}^{3} d_i^f\, \boldsymbol{e}_i \otimes \boldsymbol{e}_i \tag{6}$$

$$\boldsymbol{m}_d^i = -\underline{D}^m \cdot \boldsymbol{\omega}^i \quad \text{with} \quad \underline{D}^m = \sum_{i=1}^{3} d_i^m\, \boldsymbol{e}_i \otimes \boldsymbol{e}_i\,. \tag{7}$$

Considering the gravity force $\boldsymbol{g}^i$ the equations of motion for a single particle $\mathcal{P}^i$ are

$$m^i\, \ddot{\boldsymbol{x}}^i = \sum_{j=1}^{N_c^i} \boldsymbol{f}^{ij} + \boldsymbol{g}^i + \boldsymbol{f}_d^i\,, \tag{8}$$

$$\underline{J}^i \cdot \dot{\boldsymbol{\omega}}^i + \boldsymbol{\omega}^i \times \underline{J}^i \cdot \boldsymbol{\omega}^i = \sum_{j=1}^{N_c^i} \boldsymbol{m}^{ij} + \boldsymbol{m}_d^i\,. \tag{9}$$

Herein N_c^i is the number of contacts of $\mathcal{P}^i$, $\underline{J}^i$ is the moment of inertia with respect to the center of mass and $\boldsymbol{m}^{ij}$ is the moment of the contact force $\boldsymbol{f}^{ij}$ with respect to the center of mass.
The key-task within a DEM simulation is the solution of the equations of motion of all particles. For this explicit time integrators are applied. Here two different integration schemes are used: The third order Verlet-Leapfrog method for the translational part and the fourth order Runge-Kutta method for the rotational part. These integrators do not lead to a loss of energy and momentum during the simulation. Within the simulation every time-step is split into two main tasks: First the calculation of the contact forces between all particles and second the update of the position, velocities and accelerations of all particles according to the integration scheme. Due to the relatively complex geometry of a superellipsoid the contact determination is the most expensive part within the simulation.

3 Homogenization strategy

The macroscopic mechanical behavior of a granular material represented by the DEM should be described in terms of a standard continuum model. Hence informations resulting from the DEM simulation, i.e. the contact forces and the motion of the individual particles, are transferred to a continuum mechanical description in form of stresses and strains by an averaging procedure. First, an expression for the average Cauchy stress tensor will be derived from the inter-particle contact forces. Second, the same approach is used to derive an expression for the average linear strain tensor from the particle's motion.

3.1 Stress

Starting point of the applied homogenization approach is the definition of representative volume elements (RVEs), which serve as averaging volumes for the macroscopic quantities. Here the size d of a RVE plays an important role. Let the macroscopic body be of a characteristic length D and let the single particles have a characteristic diameter of δ. Then the scale separation

$$D \gg d \gg \delta \tag{10}$$

should hold in order that the homogenization approach is applicable. The scale separation argument is the starting point for the derivation of the average stress tensor. Denoting $\epsilon_d = d/D$ and looking at the balance of momentum of a RVE $\mathcal{R}$ inside the macroscopic body $\mathcal{B}$, the volumetric contributions are proportional to ϵ_d^3 while the surface contributions are proportional to ϵ_d^2. Therefore, in the limit of $\epsilon_d \to 0$ the volumetric contributions may be neglected leading to the equilibrium condition for a RVE

$$\int_{\partial\mathcal{R}} \boldsymbol{t}\, da = \sum_{i=1}^{N_{\partial\mathcal{R}}} \sum_{c=1}^{C^i} \boldsymbol{f}_c^i = \boldsymbol{0}\,. \tag{11}$$

Herein $N_{\partial\mathcal{R}}$ is the number of boundary particles of $\mathcal{R}$, i.e. the number of particles that are in contact with particles not belonging to $\mathcal{R}$, and C^i is the number of outside contacts of the boundary particle $\mathcal{P}^i$.
A crucial point of the homogenization approach is the reduction of the contact forces acting on a single boundary particle to a resultant force-moment pair acting in the center of mass of the particle

$$\boldsymbol{f}^i = \sum_{c=1}^{C^i} \boldsymbol{f}_c^i \quad \text{and} \quad \boldsymbol{m}^i = \sum_{c=1}^{C^i} \boldsymbol{l}_c^i \times \boldsymbol{f}_c^i\,. \tag{12}$$

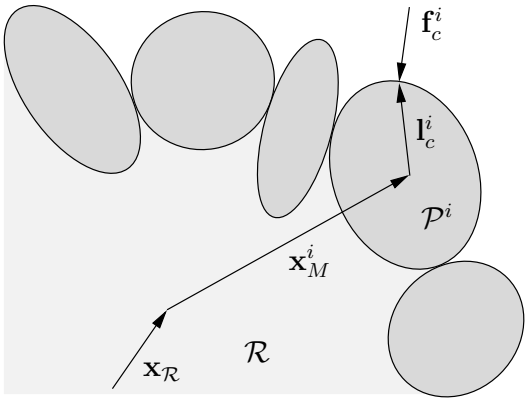

Fig. 3. Boundary particles of RVE $\mathcal{R}$ with one contact force $\boldsymbol{f}_c^i$.

In [10] and [9] the stress tensor of an extended continuum model is derived from the resultant moments. Since a standard continuum is considered here the resultant moments will not be of further interest.

In the following, div_M and grad_M denote the divergence and gradient operator with respect to the particle center positions $\boldsymbol{x}_M^i$, which can be considered as field quantity in the case of $\epsilon_\delta = \delta/d \to 0$. Using the definition of the volumetric average

$$\langle \underline{A} \rangle = \frac{1}{V_\mathcal{R}} \int_\mathcal{R} \underline{A} \, dv \tag{13}$$

and the identity

$$\underline{A}^T = \mathrm{div}_M \left(\boldsymbol{x}_M \otimes \underline{A} \right) - \boldsymbol{x}_M \otimes \mathrm{div}_M \underline{A} \tag{14}$$

one obtains an expression for the transposed average Cauchy stress tensor

$$\langle \underline{\sigma}^T \rangle = \frac{1}{V_\mathcal{R}} \int_\mathcal{R} \left[\mathrm{div}_M \left(\boldsymbol{x}_M \otimes \underline{\sigma} \right) - \boldsymbol{x}_M \otimes \mathrm{div}_M \underline{\sigma} \right] dv \, . \tag{15}$$

Application of the local form of equilibrium $\mathrm{div}\, \underline{\sigma} = \mathbf{0}$, the divergence theorem and Cauchy's theorem yields

$$\langle \underline{\sigma} \rangle = \frac{1}{V_\mathcal{R}} \int_{\partial\mathcal{R}} \boldsymbol{t} \otimes \boldsymbol{x}_M \, da \, . \tag{16}$$

Transformation into the discrete form according to (11) and (12) leads to

$$\langle \underline{\sigma} \rangle = \frac{1}{V_\mathcal{R}} \sum_{i=1}^{N_{\partial\mathcal{R}}} \boldsymbol{f}^i \otimes \boldsymbol{x}_M^i . \tag{17}$$

It can be shown (compare [2]) that under the conditions of static equilibrium and a small particle size compared to the RVE size ($\epsilon_\delta \to 0$) the average stress tensor (17) becomes symmetric and independent of the reference point $\boldsymbol{x}_\mathcal{R}$, which is used to measure the positions of the particle centers $\boldsymbol{x}_M^i$, compare Fig. 3.

3.2 Strain

A DEM simulation yields displacements and rotations of the individual particles. Using the same scheme as above this results will be transferred into a strain tensor by averaging over a RVE and transforming the resulting volumetric integral into an integral over the boundary of the RVE. In contrast to the stress calculation, where a discretization of the boundary is given naturally by the DEM simulation in form of the contact forces, the discretization has to be determined explicitly for calculation of average strains. Under the assumption of small displacements the linear strain tensor

$$\underline{\epsilon} = \frac{1}{2}\left(\mathrm{grad}_M \boldsymbol{u} + \mathrm{grad}_M^T \boldsymbol{u}\right) \tag{18}$$

will be used. Application of the identity

$$\mathrm{div}_M\left(\boldsymbol{u} \otimes \underline{1}\right) = \left(\mathrm{grad}_M \boldsymbol{u}\right) \cdot \underline{1} + \boldsymbol{u} \otimes \mathrm{div}_M \underline{1} = \mathrm{grad}_M \boldsymbol{u} \tag{19}$$

and the divergence theorem leads to

$$\langle \underline{\epsilon} \rangle = \frac{1}{2\,V_{\mathcal{R}}} \int\limits_{\partial \mathcal{R}} \left[\boldsymbol{u} \otimes \boldsymbol{n} + \boldsymbol{n} \otimes \boldsymbol{u}\right] dA\,. \tag{20}$$

As indicated by the capital letter dA all quantities in this expression are referred to the initial configuration. To evaluate this expression the boundary $\partial\mathcal{R}$ of the RVE is discretized in form of a triangular mesh with the particle centers serving as vertices, see Fig. 4. Under the assumption of a linear dis-

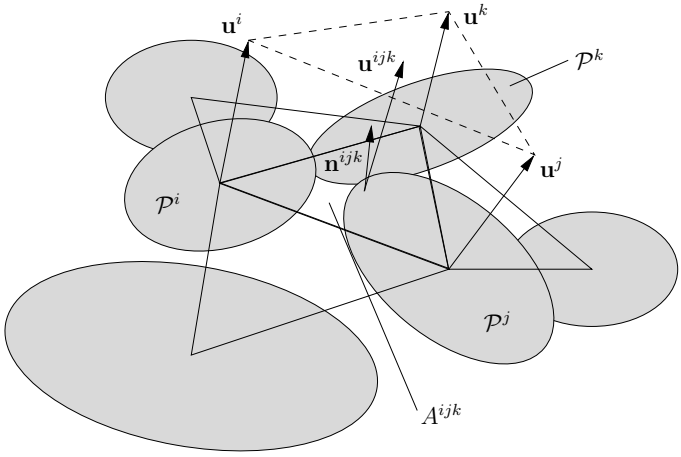

Fig. 4. Section of the triangular mesh. Triangle $\mathcal{T}^{ijk}$ is shown with its vertex and center displacements and the outward-pointing unit normal.

placement field the displacement of the center of the triangle $\mathcal{T}^{ijk}$ is given by

$$\boldsymbol{u}^{ijk} = \frac{1}{3}\left(\boldsymbol{u}^i + \boldsymbol{u}^j + \boldsymbol{u}^k\right)\,. \tag{21}$$

This yields the discretized form of (20)

$$\langle \underline{\epsilon} \rangle = \frac{1}{2\,V_{\mathcal{R}}} \sum_{ijk \in \mathbb{I}_{\mathcal{T}}} \left(\boldsymbol{u}^{ijk} \otimes \boldsymbol{n}^{ijk} + \boldsymbol{n}^{ijk} \otimes \boldsymbol{u}^{ijk} \right) A^{ijk} \tag{22}$$

where $\mathbb{I}_{\mathcal{T}}$ is the set of index triples of the triangles belonging to the discretization. Because small displacements are assumed, the discretization and all resulting quantities, i.e. the triangle areas, the unit normals and the enclosed volume, are only determined once at the beginning of a simulation.

4 RVE implementation

In order to implement RVEs into the DEM described in section 2 some technical problems have to be solved:

- Generation of a RVE
- Proper definition and discretization of the RVE boundary for strain calculation
- Estimation of the RVE volume for stress calculation

These problems are discussed below.

4.1 RVE generation

In view of the problems of boundary definition and discretization convex shaped RVEs are advantageous. A straightforward way to generate an approximately spherical shaped RVE $\mathcal{R}$ is first to choose a basis point $\boldsymbol{x}_{\mathcal{R}}$ inside the macroscopic body $\mathcal{B}$ under consideration, and second to determine all particles whose center has a smaller distance to $\boldsymbol{x}_{\mathcal{R}}$ than a given RVE radius $r_{\mathcal{R}}$. Care has to be taken that the distance of $\boldsymbol{x}_{\mathcal{R}}$ to the boundary of $\mathcal{B}$ is somewhat bigger than $r_{\mathcal{R}}$ so that the generated RVE is completely surrounded by other particles. The set of particles belonging to $\mathcal{R}$ is determined once in the beginning of the DEM simulation and kept unchanged in the aftermath.

4.2 Boundary definition and discretization

Regarding the stress calculation, the boundary particles of a RVE are defined as those particles, which are in contact with particles outside the RVE. Since there is no such definition available in the case of strain calculation, it seems straightforward to consider the same particles as boundary particles here. The derivation of the average strain tensor then yields a boundary surface that runs through the centers of these particles. Accordingly, the derivation of the stress tensor leads to a boundary surface running through all contact points of particles inside and outside $\mathcal{R}$. The problem with this approach is that it does not yield a unique surface. This is demonstrated for a two-dimensional example and the strain boundary in Fig. 5. In (a) and (b) two different ways of connecting the centers of the five boundary particles are shown. These two possible boundaries will yield different RVE volumes and boundary discretizations and therefore different averages of the macroscopic quantities.
Another argument against this approach is that the set of boundary particles

used for stress calculation changes throughout the DEM simulation while the set of particles used for strain calculation is fixed at the beginning. Thus, both sets will differ in the course of the simulation even when they are equal in the beginning.

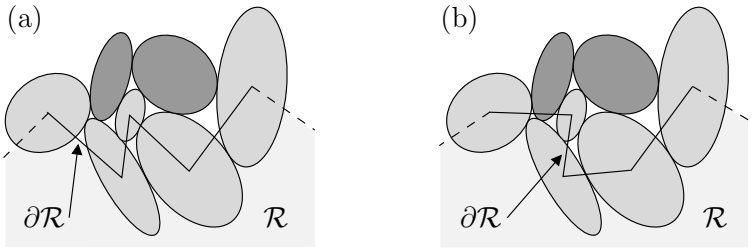

Fig. 5. Five boundary particles and two possible ways of connecting their centers of mass.

This problem is solved by using a different, well-defined set of particles for strain calculation. A convenient approach is to select those particles, whose centers specify the convex hull of all particle centers of the RVE. This choice of particles has the following advantages:

- The particles chosen all lie on the boundary of the RVE, also they do not need to have a contact partner outside the RVE.
- Because of the spherical shape of the RVEs the set of particles used for strain and stress calculation will be similar.
- There are algorithms available for computing the convex hull.

One possibility to compute the convex hull is by determining the Delaunay triangulation of the particle centers. This approach is advantageous, because it additionally yields a discretization of the boundary in form of a triangular mesh and the volume enclosed. Hence, all data needed for strain calculation can be deducted from the Delaunay triangulation. An example is presented in Fig. 6. The RVE shown consists of 76 particles, which partly can be seen in (a). The centers of the darker particles specify the convex hull. (b) shows the corresponding triangular mesh of the boundary drawn from the Delaunay triangulation. The algorithm applied here to compute the Delaunay triangulation can be found in [1].

4.3 Estimation of the RVE volume for stress calculation

As a result of the approximately spherical shape of a RVE the surface defined by the convex hull is similar to a surface which runs through the contact points of particles inside and outside of the RVE, see the two-dimensional sketch in Fig. 7. It shows the boundaries $\partial\mathcal{R}_{(1)}$ defined by the convex hull and

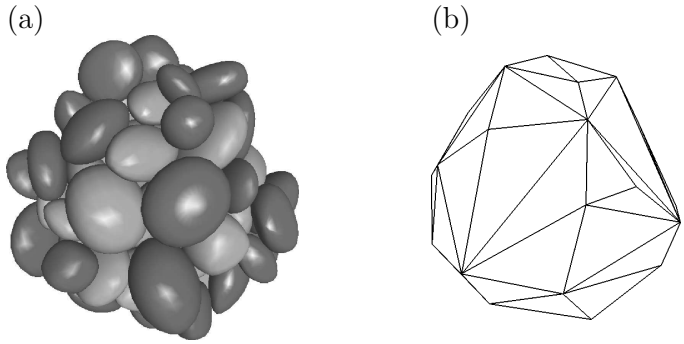

Fig. 6. RVE consisting of 76 particles. The centers of the darker particles in (a) specify the convex hull. (b) shows the corresponding triangular mesh.

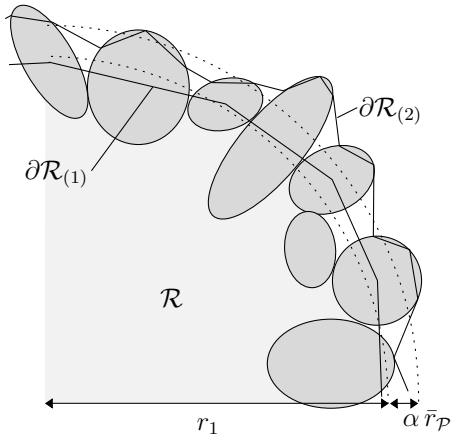

Fig. 7. Section of a two-dimensional RVE with only particles near the boundary displayed. $\partial\mathcal{R}_{(1)}$ is defined by the convex hull, $\partial\mathcal{R}_{(2)}$ runs through the contact points. The two circles enclose the same area as the boundaries.

$\partial\mathcal{R}_{(2)}$, which runs through the contact points. The idea now is to estimate the volume V_2 enclosed by $\partial\mathcal{R}_{(2)}$ through the known volume V_1 enclosed by $\partial\mathcal{R}_{(1)}$. Therefor the radius r_1 of a sphere with volume V_1 is determined. The corresponding radius r_2 now has to be bigger than r_1, because $\partial\mathcal{R}_{(2)}$ mainly runs outside of $\partial\mathcal{R}_{(1)}$. The difference between the radii should lie in the range of the average radius $\bar{r}_{\mathcal{P}}$ of the particles belonging to $\mathcal{R}$. Hence the estimation

$$r_2 = r_1 + \alpha\,\bar{r}_{\mathcal{P}} \quad \text{with} \quad \alpha \in [0,1]$$

is used. The factor α has to be independent of the ratio of particle size and RVE size, but may depend on particle shape and size distribution. It can be determined by comparing the RVE-based stresses with macroscopic results. For the particle sample described in section 5.1 numerical experiments showed, that $\alpha = 0.3$ is a good value.

5 Validation of the homogenization strategy

Two kinds of DEM simulations are used to validate the proposed homogenization strategy. First, a compression test, and second, a shear test of a cuboid box filled with particles are performed.

5.1 Model used for DEM simulations

Since the results of the DEM simulations are not compared quantitatively with results of tests on real granular materials, no units will be used in the following. The model for the numerical tests consists of 1609 particles, which are surrounded by a cuboid box with the dimensions $21.0 \times 21.0 \times 23.6$, see Fig. 8. It was produced by creating 1530 superellipsoids whose centers lie on

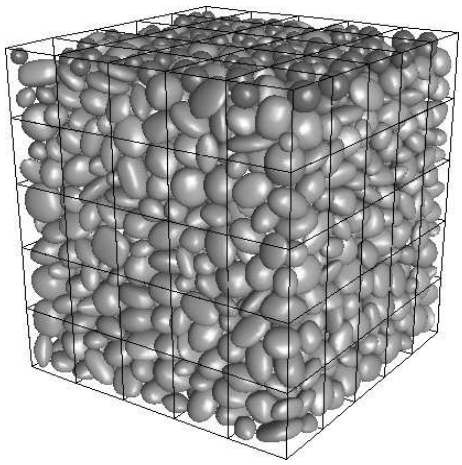

Fig. 8. Model used for DEM simulations. The brighter particles are superellipsoids. The darker particles are spheres, that were added in order to raise the number of particle-box contacts at the upper side of the surrounding box.

a regular grid. The distance of adjacent grid points was chosen big enough to prevent the superellipsoids from overlapping. The five parameters of each superellipsoid were selected randomly and equally distributed out of the intervals listed below:

parameter	interval	average
a, b, c	$[0.5, 1.5]$	1.0
m, n	$[0.7, 1.3]$	1.0

Under the influence of gravity the superellipsoid particles fell into the box resulting in the package shown in Fig. 8. Finally 69 spheres were fit into the space between the top superellipsoids and the upper side of the surrounding box in order to obtain a similar number of particle-box contacts here like at

the other sides of the box. The radius of the spheres lie in the interval $[0.5, 1.5]$. The volume of the particle package generated by this procedure makes up 63% of the volume of the surrounding box.

5.2 RVEs and interpretation of results

Eight RVEs, see Fig. 9, were selected to measure the macroscopic quantities. Each was generated with a radius $r_{\mathcal{R}} = 5$, resulting in an average number of about 80 particles. Since the numerical tests performed yield homogeneous macroscopic strains, the single RVEs are expected to yield similar results. Therefore, the results are evaluated by calculating average values with corresponding error bars. Since the average of a quantity X over a RVE is denoted by $\langle X \rangle$ the average of $\langle X \rangle$ over all RVEs is denoted by $\langle\langle X \rangle\rangle$. The error bars are computed as

$$\left[\langle\langle X \rangle\rangle - \frac{\sigma\left(\langle X \rangle\right)}{\sqrt{N_{\mathcal{R}}}}, \langle\langle X \rangle\rangle + \frac{\sigma\left(\langle X \rangle\right)}{\sqrt{N_{\mathcal{R}}}} \right],$$

in which $\sigma\left(\langle X \rangle\right)$ is the standard deviation and $N_{\mathcal{R}}$ is the number of RVEs. In addition, macroscopic stress values are calculated by applying the homogenization approach to the whole particle sample. The contact forces between the particles and the surrounding box are then related to the box volume.

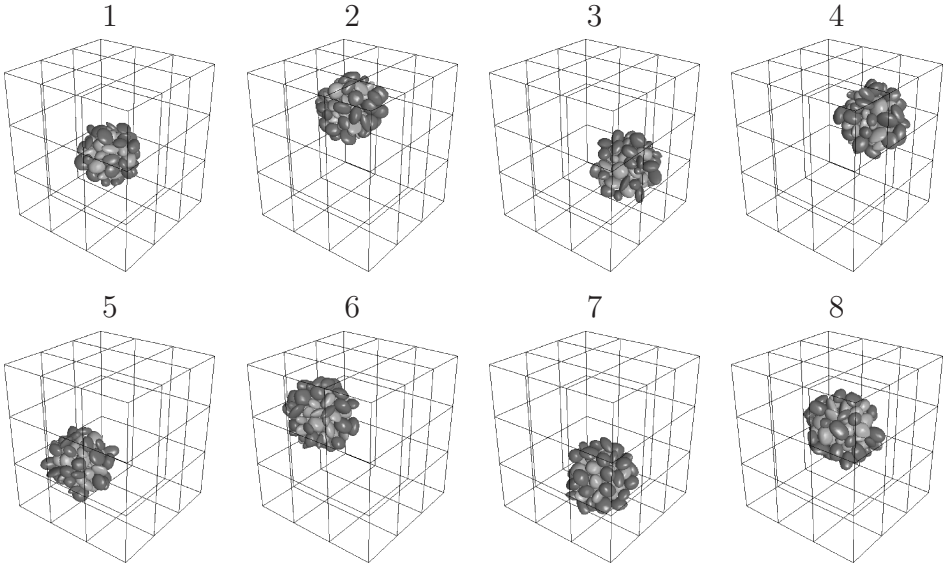

Fig. 9. Eight RVEs used for calculation of macroscopic quantities.

5.3 Compression test

The particle sample is compressed in the vertical X_3 direction by a strain driven simulation resulting in the macroscopic linear strain tensor

$$\underline{\epsilon} = -\lambda\, c_{\text{end}}\, \boldsymbol{e}_3 \otimes \boldsymbol{e}_3\,.$$

The final compression $c_{\text{end}} = 0.1$ is applied in 100 steps yielding a displacement of the upper box side of 0.023 in every loading step. The DEM parameters used are listed in the following table:

Δt	c^N	c^T	μ	d_i^f	d_i^m	N_{relax}
10^{-4}	10^6	10^6	0.5	10	5	1500

Herein N_{relax} is the number of time-steps performed after each loading step in order to obtain a state near static equilibrium of the particle sample. The stress and strain values are always calculated directly before the next loading step.
Under the loading process described above the particle sample shows a linear elastic behavior, see the results in terms of average strains and stresses in Fig. 10. Fig. 10 (a) shows the average normal strains vs. the macroscopic principle

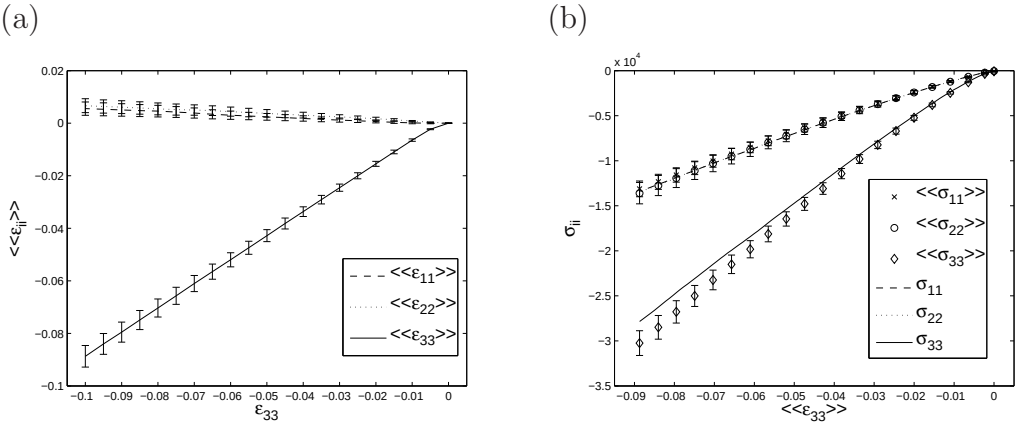

Fig. 10. Results of the compression test. Normal strains vs. macroscopic principle strain ϵ_{33} (a) and normal stresses vs. principle strain $\langle\langle\epsilon_{33}\rangle\rangle$ (b).

strain ϵ_{33}. The RVE average $\langle\langle\epsilon_{33}\rangle\rangle$ is in good agreement with ϵ_{33}. The average normal strains perpendicular to the loading direction rise until a final value of about 0.5%, while the values of shear strains are negligible. In Fig. 10 (b) the average normal stresses are compared with the macroscopic normal stresses computed from the particle-box contact forces. All components show a linear behavior and thus a good agreement of RVE and macroscopic values. The value of the ratios $\langle\langle\sigma_{11}\rangle\rangle/\langle\langle\sigma_{33}\rangle\rangle$ and $\langle\langle\sigma_{22}\rangle\rangle/\langle\langle\sigma_{33}\rangle\rangle$ of about 0.5 is reasonable compared to results of geomechanical tests.

Furthermore the influence of DEM parameters was analyzed. For this purpose the compression test was first repeated with the penalty parameters c^N and c^T set to half and double of the original values. The results of these tests depicted that the average stresses are directly proportional to the penalty parameters. This is a reasonable result because c^N and c^T act as elastic constants in the contact formulation of the DEM.
To analyze the influence of the coefficient of friction μ the test was repeated with μ set to 0.25, 0.1 and 0. The final compression was reduced to 4% for these tests. For analyzation of the results the principal stresses

(a) (b)

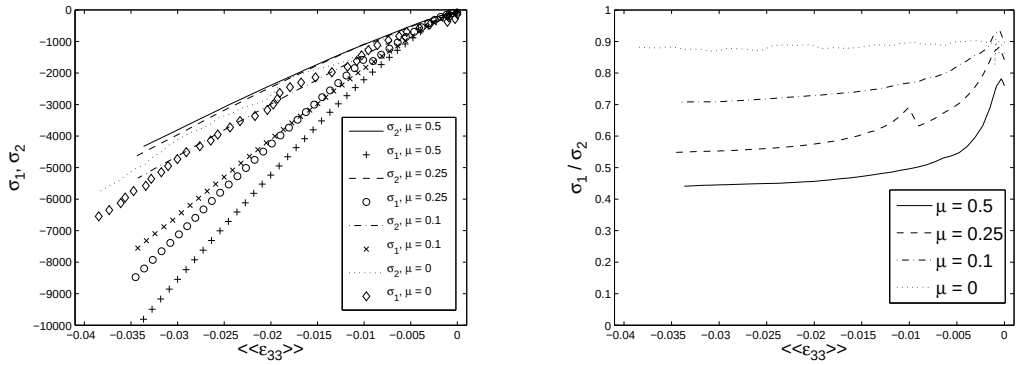

Fig. 11. Influence of the coefficient of friction μ on the principal stresses (a) and their ratio (b).

$$\sigma_1 = \langle\langle\sigma_{33}\rangle\rangle \quad \text{and} \quad \sigma_2 = \frac{1}{2}\left[\langle\langle\sigma_{11}\rangle\rangle + \langle\langle\sigma_{22}\rangle\rangle\right] \tag{23}$$

are defined. In Fig. 11 the principal stresses (a) and their ratio (b) are plotted against $\langle\langle\epsilon_{33}\rangle\rangle$ for the different values of μ. A decrease of μ yields a decrease of σ_1 and an increase of σ_2. That means the system tends towards a hydrostatic state with decreasing μ. While the ratio σ_1/σ_2 is about 0.5 for $\mu = 0.5$ it is about 0.9 for $\mu = 0$.

5.4 Shear test

The initial state of the particle sample used for the shear test is already compressed by an amount of c in the X_3 direction. This models a normal pressure in vertical direction. Now the sample gets sheared in the X_1,X_3 plane by a strain driven simulation yielding a macroscopic linear strain tensor

$$\underline{\epsilon} = \frac{1}{2}\,\lambda\,\gamma_{\text{end}}\,(\boldsymbol{e}_1 \otimes \boldsymbol{e}_3 + \boldsymbol{e}_3 \otimes \boldsymbol{e}_1) - c\,\boldsymbol{e}_3 \otimes \boldsymbol{e}_3\,.$$

The final shearing strain $\gamma_{\text{end}} = 0.2$ is applied in 50 steps leading to a displacement of the upper box side in X_1 direction of about 0.1 in every loading step. The DEM parameters have been retained unchanged from the compression test.

First the average strains are compared with the macroscopic strains, see Fig. 12 (a) and (b). Here the compression of the initial state is neglected, hence the average normal strains all start at zero. $\langle\langle\epsilon_{11}\rangle\rangle$ rises to a final value of about 1%, $\langle\langle\epsilon_{22}\rangle\rangle$ decreases to about -1% and $\langle\langle\epsilon_{33}\rangle\rangle$ does not show a clear direction. The error bars of all normal strains are relatively large. The average shear strains show the expected behavior. The main shear strain component is in good agreement with the macroscopic value and the other components are negligible.

Looking at the results for the stresses in Fig. 12 (c) and (d) one can see that

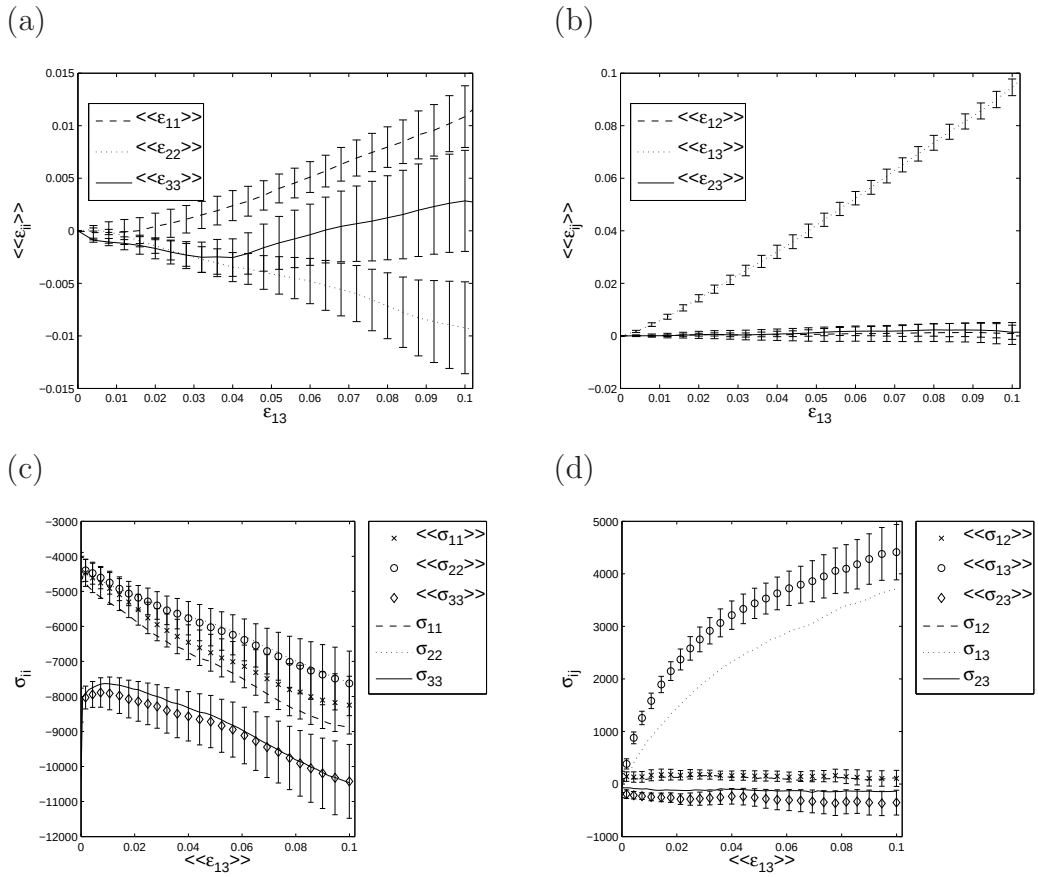

Fig. 12. Results of the shear test. Normal (a) and shear (b) strains vs. macroscopic shear strain ϵ_{13}. Normal (c) and shear (d) stresses vs. average shear strain $\langle\langle\epsilon_{13}\rangle\rangle$.

there is an approxiametly linear rise of the normal stresses with the average main shear strain. Again the macroscopic and RVE values are in good agreement. The main shear stress shows a nonlinear behavior with the slope of the curve decreasing until a shear strain of about 4% and then remaining constant. Here the RVE and macroscopic values differ by about 30%. The other shear

stresses are negligible.
Finally, the influence of the initial compression and the coefficient of friction on the main shear stress was analyzed. Therefor the shear test was performed with initial compressions of $c = 0.04$, 0.06 and 0.08 and with a compression of $c = 0.04$ and the coefficient of friction set to $\mu = 0.25$. The results are depicted in Fig. 13. A rise of the initial compression yields higher shear stresses.

(a) (b)

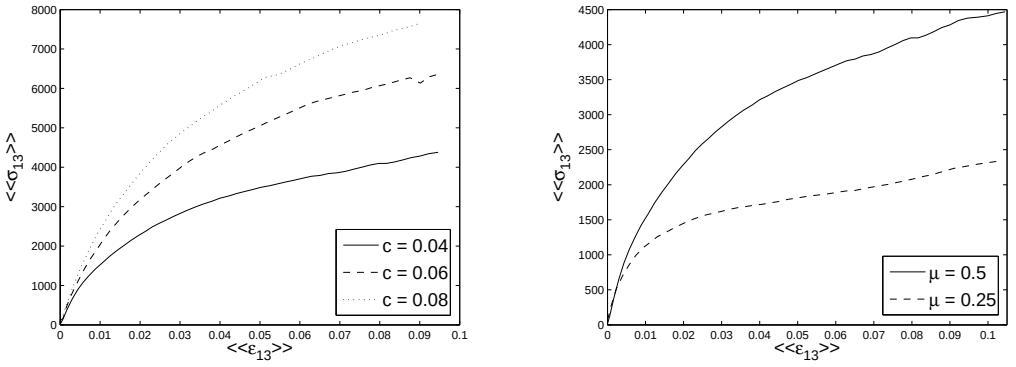

Fig. 13. Influence of the initial compression c (a) and the coefficient of friction μ (b) on the main shear stress $\langle\langle\sigma_{13}\rangle\rangle$.

Thereby the initial and final slope of the three shear stress curves remain approximately unchanged. The reduced local friction coefficient μ yields smaller shear stresses. Additionally the final slope of the shear stress curve decreases while the initial slope is not influenced.

6 Fitting the results to a macroscopic constitutiv equation

The particle sample, described in section 5.1, shows a material response which can be modeled using a standard elasto-plastic material. The results of the compression and shear tests in the form of stress-strain curves are used to identify the parameters of the material model. The particle sample acted linear elastic under compression. Under shearing it showed a nonlinear behavior with higher pressures yielding higher shear stresses. This motivates the use of the Drucker-Prager plasticity model which is based on the yield function

$$f\left(\underline{\sigma}\right) = \|\mathrm{dev}\,\underline{\sigma}\| + \frac{1}{\sqrt{6}}\,\mu\ \mathrm{tr}\,\underline{\sigma} - Y_0 \leq 0\,.$$

Herein the parameter Y_0 describes the cohesion of the material. Since there are no cohesion-forces in the DEM used, Y_0 is set zero. The elastic part of the material behavior is described by Hooke's law.
First, the elastic parameters are fit to the results of the compression test. This yields a bulk modulus of $K = 235604.5$ and a shear modulus of $G = 84936.3$. Fig. 14 (a) shows that the resulting normal stresses mainly lie within the error bars of the RVE stresses. Next, the elastic constants are used to fit

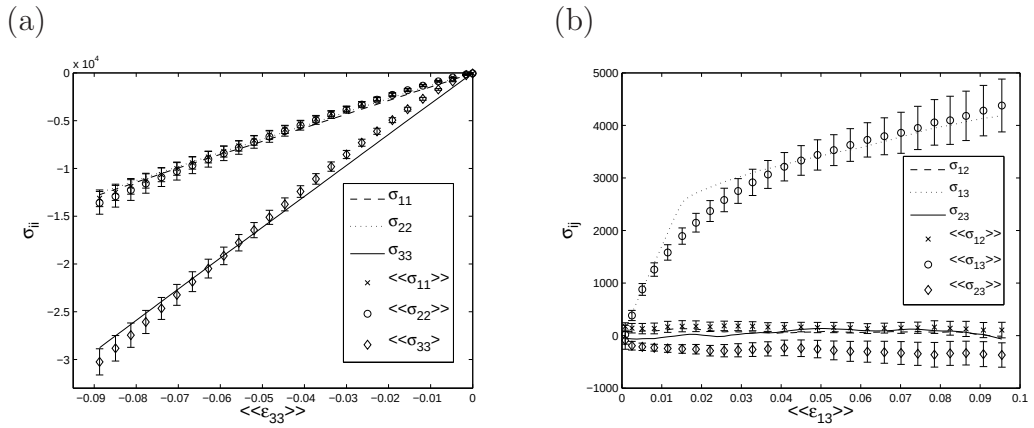

Fig. 14. Elasto-plastic material fit to the RVE stress strain curves. Fitting of the bulk and shear modulus to the results of the compression test (a) and fitting of the plastic constant μ to the results of the shear test (b).

the plastic constant μ to the results of the shear tests. Small strains were assumed so that the total strain could be split additively into elastic and plastic parts. The stresses and plastic strains are then computed incrementally using a predictor-corrector method with a non-associated flow rule resulting in pure deviatoric plastic strains. Thereby the standard approach has to be modified to account for an aspect of the particle sample's reaction under shear loading: There is an increase in volumetric strain combined with an increase in pressure, see Fig. 12 (a) and (c). Although this can't be reproduced by the combination of Drucker-Prager model and Hooke's law, the yield function still

seems reasonable since it only depends on stresses. This problem is handled by modifying the predictor-corrector method in such a way, that only the shear stresses are calculated from the deviatoric strains while the normal stresses are simply set to the RVE values. Application of this procedure to the shear test with an initial compression of $c = 0.04$ yields a plastic constant of $\mu = 0.59$. A comparison of the shear stresses is shown in Fig. 14 (b). The stresses calculated by the modified predictor-corrector method mainly lie within the error bars of the RVE stresses and there is a good agreement of the initial and final slopes. Usage of the shear tests with $c = 0.06$ and $c = 0.08$ leads to plastic constants of $\mu = 0.56$ and $\mu = 0.53$ respectively, which are slightly decreasing when compared to the first result.

7 Conclusion

In the present paper a homogenization approach for granular materials is applied to a three-dimensional DEM. Microscopic quantities on the particle scale are related to macroscopic quantities by volumetric averaging over representative volume elements (RVEs). The resulting expression for the stress tensor consists of a summation over the inter-particle contact forces on the RVE boundary. The corresponding strain tensor is obtained by an integration over the displacement field defined by the mass centers of the particles on the RVE boundary. This boundary is defined as the convex hull of the particle centers. The determination of the convex hull by a Delaunay triangulation yields a discretization of the boundary and the enclosed volume right away.
The homogenization strategy is then validated by means of strain driven DEM simulations of a compression and a shear test of a cuboid sample of cohesionless particles. Because of the homogeneity of the applied deformations the values of the macroscopic quantities calculated from the RVEs are averaged over all RVEs for evaluation. The resulting strain values are in good agreement with the macroscopic values. The resulting stresses are reasonable and in good agreement with macroscopic values, computed from particle-boundary contact forces. The particle sample thereby shows a linear elastic behavior under compression and a nonlinear pressure-dependent behavior under shear loading. The influence of some DEM parameters on this response is made clear to some extent. Further analyzations of the influence of particle shape and particle size distribution would be interesting future tasks.
Finally, it is shown that the macroscopic behavior of the particle sample could be well described by a simple Drucker-Prager soil model, when a modification is applied, that accounts for the dilatancy effect. The elastic and plastic parameters of the model are fit to the stress-strain curves of the compression and shear test, resulting in reasonable values. Hence, the developed method is applicable to granular frictional materials.
Future work has to include testing of real granular assemblies in order to be able to use the developed scheme for quantitative predictions using an eventually more refined constitutive equation at the macroscopic level.

References

[1] C. B. Barber, D. P. Dobkin and H. T. Huhdanpaa; *The quickhull algorithm for convex hulls*; in: ACM Transactions of Mathematical Software; 22(4) :469–483; 1996

[2] J. P. Bardet and I. Vardoulakis; *The asymmetry of stress in granular media*; in: International Journal of Solids and Structures; 38(2) :353–367; 2001

[3] A. H. Barr; *Superquadrics and Angle-Preserving Transformations*; in: IEEE Computer Graphics and Applications; 1(1) :11–23; 1981

[4] P.W. Cleary, N. Stokes and J. Hurley; *Efficient collision detection for three dimensional super-ellipsoid particles*; Proceedings of 8th International Computational Techniques and Applications Conference CTAC97, Adelaide; 1997

[5] P. A. Cundall; *Formulation of a three-dimensional distinct element model. I: A scheme to detect and represent contacts in a system composed of many polyhedral blocks*; in: International Journal of Rock Mechanics and Mining Sciences; 25(3) :107–116; 1988

[6] P. A. Cundall; *A discontinuous future for numerical modelling in geomechanics?*; in: Geotechnical Engineering; 149(1) :41–47; 2001

[7] P. A. Cundall and R. D. Hart; *Numerical modelling of discontinua*; in: Engineering Computations; 9(2) :101–113; 1992

[8] P. A. Cundall and O. D. L. Strack; *A discrete numerical model for granular assemblies*; in: Geotechnique; 29 :47–65; 1979

[9] G. A. D'Addeta; *Discrete models for cohesive frictional materials*; PhD thesis; University of Stuttgart, Institute of Structural Mechanics; 2004

[10] G. A. D'Addetta, E. Ramm, S. Diebels and W. Ehlers; *A particle center based homogenization strategy for granular assemblies*; in: Engineering Computations; 21(2/3/4) :360–383; 2004

[11] J.F. Favier, M.H. Abbaspour-Fard, M. Kremmer and A.O. Raji; *Shape representation of axi-symmetrical, non-spherical particles in discrete element simulation using multi-element model particles*; in: Engineering Computations; 16(4) :467–480; 1999

[12] J.-A. Ferrez; *Dynamic triangulations for efficient 3D simulation of granular materials*; PhD thesis; Ecole Polytechnique Federale de Lausanne; 2001

[13] J. Ghaboussi and R. Barbosa; *Three-dimensional discrete element method for granular materials*; in: International Journal for Numerical and Analytical Methods in Geomechanics; 14(7) :451–472; 1990

[14] S. Johnson, J. R. Williams and B. Cook; *Contact resolution algorithm for an ellipsoid approximation for discrete element modeling*; in: Engineering Computations; 21(2/3/4) :215–234; 2004

[15] X. Lin and T.-T. Ng; *A three-dimensional discrete element model using arrays of ellipsoids*; in: Geotechnique; 47(2) :319–329; 1997

[16] C. Miehe and J. Dettmar; *A framework for micro-macro transitions in periodic particle aggregates of granular materials*; in: Computer Methods in Applied Mechanics and Engineering; 193(3) :225–256; 2004

[17] E. Rougier, A. Munjiza and J. P. Latham; *Shape selection menu for grand scale discontinua systems*; in: Engineering Computations; 21(2/3/4) :343–359; 2004

[18] A. M. Sallam; *Studies on Modeling Angular Soil Particles Using the Discrete Element Method*; PhD thesis; University of South Florida, College of Engineering; 2004

[19] E. Tijskens, J. De Baerdemaeker and H. Ramon; *Strategies for contact resolution of level surfaces*; in: Engineering Computations; 21(2/3/4) :137–150; 2004

[20] J. M. Ting, L. Meachum and J. D. Rowell; *Effect of particle shape on the strength and deformation mechanisms of ellipse-shaped granular assemblages*; in: Engineering Computations; 12(2) :99–108; 1995

[21] C.-Y. Wang, C.-F. Wang and J. Sheng; *A packing generation scheme for the granular assemblies with 3D ellipsoidal particles*; in: International Journal for Numerical and Analytical Methods in Geomechanics; 23(8) :815–828; 1999

[22] J. R. Williams and A. P. Pentland; *Superquadrics and modal dynamics for discrete elements in interactive design*; in: Engineering Computations; 9(2) :115–127; 1992